CDF note 9650

First measurement of the single top production cross section in the $\not\!\!E_T$ plus jets sample

The CDF Collaboration
URL http://www-cdf.fnal.gov
(Dated: January 15, 2009)

Top quarks are produced mostly in pairs at the Tevatron through the strong force. The production of one top quark per process is allowed through electroweak processes, with its cross section being half the size of the pair production. In addition, the less distintinctive signature makes it much harder to observe. Tevatron experiments looked until now only in events where one high energy electron or muon has been identified, in order to suppress the huge QCD background and achieve a reasonable signal over background ratio. We look here for the first time at events where no electron or muon has been identified, or tau leptons decay hadronically and are reconstructed as calorimetric jets. Multivariate analysis techniques are used to discriminate the single top signal against the dominant backgrounds, and we use a likelihood profile of this discriminant to measure the production cross section of single top events, reaching the expected sensitivity of 1.4σ. Once looking at the first $2.1\,\mathrm{fb}^{-1}$ of data recorded by CDF, we measure a cross section of $\sigma^{obs}_{s+t} = 4.9^{+2.5}_{-2.2}$ pb with a sensitivity of 2.1σ. We also measure the V_{tb} element of the CKM matrix: $|V_{tb}| = 1.24^{+0.34}_{-0.29} \pm 0.07$(theory).

Preliminary Results for Winter 2009 Conferences

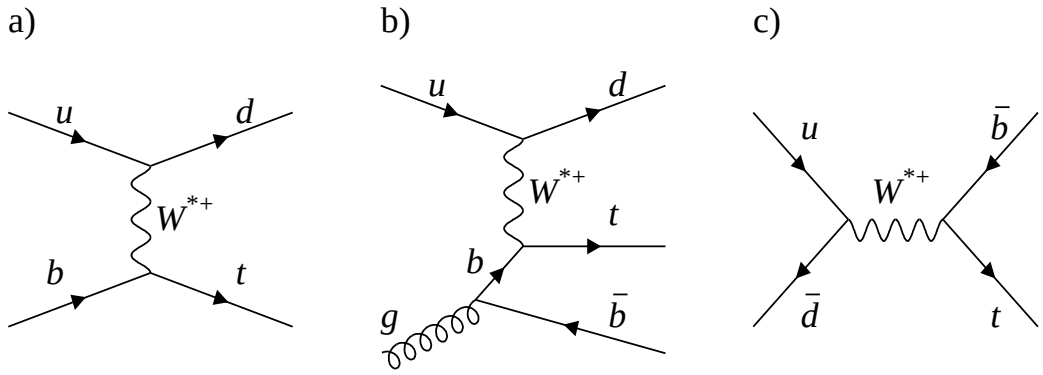

FIG. 1: Representative Feynman diagrams of single top quark production. Figures (a) and (b) are t-channel processes, and figure (c) is the s-channel process.

I. INTRODUCTION

This note describes a measurement of the single top production cross section in $\bar{p}p$ collisions at $\sqrt{s} = 1.96$ TeV with the CDF II detector at the Fermilab Tevatron. The Standard Model predicts that the top quark decays to a W boson and a b quark almost 100% of the times, and the W subsequently decays hadronically or leptonically. We are interested in those events where the W decays leptonically but the electron or muon escapes detection, or where the tau is reconstructed as a jet, yielding a final state of two b-quark jets, no leptons and large missing transverse energy ($\not\!\!E_T$, from W decay). The presence of b-jets allows us to use b-tagging algorithms to further suppress backgrounds.

Single top is produced mostly through the t-channel with a cross section of 1.98 pb, or through the s-channel with a cross section of 0.88 pb [1]. Figure 1 shows the representative Feynman diagrams. We look here at events discarded by other analysis, i.e. events where there are no identified leptons, thus relying solely on the signature of high P_T jets and $\not\!\!E_T$. The contributions from the various decay modes of the W boson in single top events are shown in table I.

This sample, being statistically independent from the one used till now by CDF, provides independent measurements the single top cross-section and V_{tb}, which can be regarded as a consistency check. Moreover, these measurements can be combined to the existing measurements to increase the precision in the determinations of these two quantities.

The CDF II detector is described in detail in [2].

s-channel	$W \to e\nu$	$W \to \mu\nu$	$W \to \tau\nu$
all events	19%	30%	51%
2 jet events	20%	34%	46%
3 jet events	17%	24%	59%

(a) s-channel

t-channel	$W \to e\nu$	$W \to \mu\nu$	$W \to \tau\nu$
all events	19%	29%	51%
2 jet events	21%	32%	47%
3 jet events	17%	23%	61%

(b) t-channel

TABLE I: Contributions to 2/3 jet events from different leptonic decay modes of the W boson in single top events

II. DATA SAMPLE & EVENT SELECTION

This analysis is based on a integrated luminosity of 2.1 fb^{-1} collected with the CDF II detector. The data are collected with a $\not\!\!E_T$ plus two jets trigger [3].

Jets are reconstructed from energy depositions in the calorimeter towers using a jet clustering cone algorithm with a cone size of radius $R = \sqrt{(\Delta\phi)^2 + (\Delta\eta)^2} = 0.4$. Jet energies are corrected to account for effects that cause mismeasurements in the jet energy such as non-linear calorimeter response, multiple beam interactions, or displacement of the event vertex from the nominal position. We further correct jet energies by reconstructing their four-momenta according to the H1 prescription [4]. Both the magnitude and the direction of $\not\!\!E_T$ are recalculated after correcting the energies of jets.

The trigger efficiency is obtained from data and is used to scale the Monte Carlo signal and background samples to correct for event loss during data taking. The overall efficiency of the online event selection is parametrized by the offline corrected $\not\!\!E_T$ and applied on the Monte Carlo samples providing a proper scaling for the simulated events.

From this inclusive dataset we select events offline with the following requirements (jets are sorted according to their energies):

- $\not\!\!E_T > 50$ GeV, to avoid trigger inefficiencies ;
- the two leading jets are within $|\eta| < 2.0$, with at least one jet being central $|\eta| < 0.9$;
- leading jet $E_T > 35$ GeV and second leading jet $E_T > 25$ GeV ;
- $\Delta R(1^{\text{st}}\text{ jet}, 2^{\text{nd}}\text{ jet}) > 1.0$;
- events with 4 or more jets with $E_T > 15$ GeV in $|\eta| < 2.4$ region are rejected.

We also accept events with three jets in this channel. The main motivation is to accept events from the NLO t-channel diagram. The third jet might also be coming from hard radiation from the final state quarks, as well as from hadronic tau decays from $W \to \tau\nu$. Events passing all of the above selections form the *event pre-selection*, also called *pre-tag sample*.

As a way to get a better estimate of the event true $\not\!\!E_T$, we calculate the $\not\!\!p_T^{tr}$, which is defined as negative vector sum of charged particle track P_T. For true $\not\!\!E_T$ events, $\not\!\!p_T^{tr}$ is highly correlated with Calorimeter $\not\!\!E_T$, while for QCD multijet events with mismeasured jets it is not. Thus, $\not\!\!p_T^{tr}$ provides an additional handle to separate mismeasurements from real $\not\!\!E_T$ events.

A. Tagging algorithms

In order to improve the signal to background further, we need to identify jets originating from a b quark. We do so by employing both the SecVTX [5] and JetProb [6] b-tagging algorithms. We subdivide the sample into three orthogonal tagging categories:

- exactly one jet is tagged by the SecVTX algorithm at the tight operating point;
- both jets are tagged by the tight SecVTX algorithm;
- one jet is tagged by the tight SecVTX algorithm and the other jet by the JetProb algorithm with $< 5\%$ probability.

B. A neural network (NN) to remove QCD multijet production

The main background in this search is the QCD production of two or three jets. We investigated the dynamic of the events in the sample using a data-driven QCD multijet production model (see below). Looking at a large set of variables, we keep here only the ones for which QCD has a very different behaviour with respect to the signal and the remaining backgrounds; the idea is that we will remove events very much not signal-like with a NN, and then use a second NN to discriminate the surviving, more signal-like backgrounds.

We train a mixture of 50% single top s-channel events and 50% t-channel against pre-tag data times tag rate probability (for modeling QCD multijet). We use a Multi Layer Perceptron (MLP), which is a simple feed-forward network, as implemented inside the TMVA [7] package. We will refer to the output of this NN as QCDNN .

We used the following 15 variables to train the NN:

- Absolute amount of the missing transverse momentum, $\not\!\!p_T^{tr}$;
- Absolute amount of the missing transverse energy, $\not\!\!E_T$;
- Difference in ϕ between missing transverse energy $\not\!\!E_T$ and missing transverse momentum $\not\!\!p_T^{tr}$, $\Delta\phi(\not\!\!E_T, \not\!\!p_T^{tr})$;
- Maximum of the difference in the R space between two jets, taking two jets at the time;
- Minimum of the difference in ϕ between the $\not\!\!E_T$ and each jet j_i, considering all two or three $(\not\!\!E_T, j_i)$ pairings;

- Minimum of the difference in ϕ between the $\not\!\!P_T^{tr}$ and the jets, considering all two or three $(\not\!\!P_T^{tr}, j_i)$ pairings;
- Maximum of the difference in ϕ between two jets directions, taking two jets at the time;
- Ratio of $\not\!\!H_T$ (vector sum of tight jet E_T) and the $\not\!\!E_T$;
- $\Delta\phi$ between the direction of the leading jets in two-jet rest frame and the direction of the boost;
- $\not\!\!E_T/H_T$: $\not\!\!E_T$ over scalar sum of the two leading jets MET;
- $\not\!\!E_T$ significance : $\not\!\!E_T$ over square root of sum E_T (all calorimetric activity);
- Invariant mass of $\not\!\!E_T$, j_1 and j_2;
- Z$(j_{1(2)})$: Ratio of the sum of Pass 1 track P_Ts to the $P_T(j_{1(2)})$;
- Event sphericity : S $= 1.5 \times(\lambda_2 + \lambda_3)$, where $\lambda_1 \geq \lambda_2 \geq \lambda_3$ are the eigenvalues of the sphericity tensor.

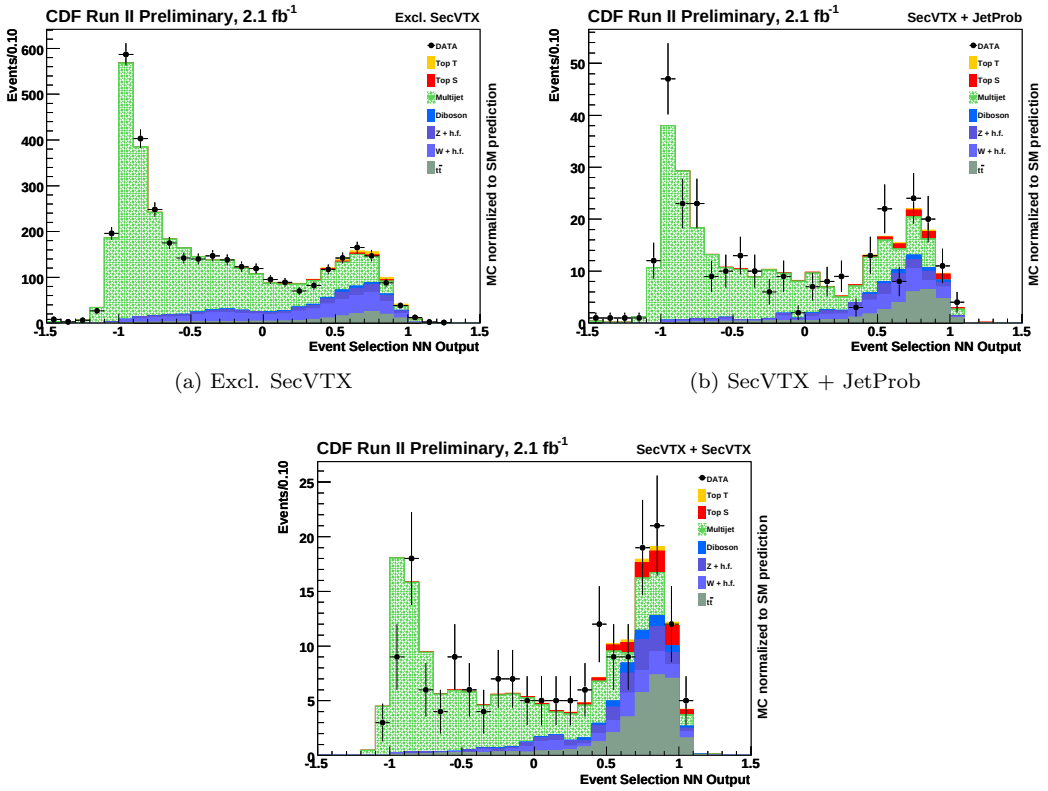

(a) Excl. SecVTX

(b) SecVTX + JetProb

(c) SecVTX + SecVTX

FIG. 2: QCDNN output for events passing our event pre-selection

The QCDNN output is shown for all tagging categories in the pre-selection region in figure 2 and in several control regions (defined in section IV) on the CDF public web-page of this analysis [10]. We cut the output of the QCDNN to define the signal region by keeping those events with QCDNN > -0.1.

III. SIGNAL AND BACKGROUND MODELING

A. Signal Modeling

The signal Monte Carlo samples were generated with MadGraph/MadEvent with the parton showering performed by Pythia [8] and reconstructed with CDF-soft version 6.1.4mc set to realistic (run-dependent) mode. The single top processes were generated for a top mass of 175 GeV.

B. Background Modeling

The final state we are interested in consists of two b-quark jets, no leptons and large $\not\!\!E_T$. There are numerous Standard Model processes that can mimic this signature. In this section, we list all the backgrounds considered in the analysis.

The most significant background at the first stage of the analysis are the QCD multijet processes. QCD jet production has a large cross-section ($\sim \mu b$), which is about 7 orders of magnitude greater than the signal before requiring the first b-tag. Although, these processes generally do not have intrinsic $\not\!\!E_T$, mismeasured jets do cause imbalance in the total transverse energy, by which the QCD events can pass the basic selection cuts if one of the jets is mis-tagged. Furthermore, QCD b-quark pair production yields taggable jets and if one b undergoes a semi-leptonic decay, large $\not\!\!E_T$ arises. In both cases, the $\not\!\!E_T$ tends to be aligned parallel or anti-parallel to the first or second most energetic jet. This topology is one of the most effective devices against the QCD background.

To estimate the QCD background from data we have developed a Tag Rate Matrix (TRM) method. This allows us to estimate not only heavy flavour QCD production, but also processes with a light flavour jet falsely tagged as a b-quark. Both of these backgrounds are treated together in the following and are referred to as QCD multijet production. In order to estimate the multijet background in the single-tagged (double-tagged) sample we measure the probability to tag one (two) jet(s) from the *pre-tag* (single-tagged) sample (section II). The tag rate probabilities are parameterized as a function of:

- transverse energy of the jet ;
- pseudo-rapidity of the jet $|\eta|$;
- event H_T , which is defined as a scalar sum of all jets in the event ;
- jet Z , which is defined as a ratio of the sum of good quality tracks in the jet to the jet P_T. This quantity provides a handle to separate light flavour jets from heavy flavour jets.

The matrix is measured in subsample of $\not\!\!E_T$+jets dataset, which is orthogonal to the final signal sample, and is defined with the following selections:

- all leptons are vetoed using loose lepton identifications ;
- azimuthal angular separation $\Delta\phi(2^{\rm nd}$ jet,$\not\!\!E_T) \leq 0.4$;
- 50 GeV $< \not\!\!E_T <$ 70 GeV.

To avoid double counting of events from other processes, we apply the matrix to the Monte Carlo simulations and subtract their contribution from the multi-jet background.

The rest of the backgrounds are determined with Monte Carlo simulation using Pythia [7]. Top pair production yields a significant contribution to the background in the signal region. Due to the large mass and the semi-leptonic decay of the top, these events are energetic, bear large $\not\!\!E_T$ and high jet multiplicity. In the di-boson samples, the bosons decays are inclusive. In the W/Z + jets samples, the bosons are forced to decay into leptons, or b-quarks. The electroweak backgrounds thus include the following processes: W to leptons + h.f., Z to leptons + h.f., WW/WZ/ZZ inclusive decays. We check our modeling of the data-sample for all tagging categories in three control regions, defined below.

C. Multijet Background Normalization

In order to estimate the backgrounds originating from QCD heavy flavour multijet production, as well as falsely tagged light flavour jet production, we use the Tag Rate Matrix method described above. This method provides us with an excellent model describing the shapes of the backgrounds very well. We test the multijet background model performance in terms of reproducing the shape of the observed distributions in CDF data in a QCD Control Region and a Electroweak/Top Control Region (the control regions are defined below).

The normalization of the expected background is not well predicted, and a scaling factor needs to be determined. In order to constrain the expected rates of these backgrounds we use a signal-like, QCD-rich control region. The scaling factor is determined in a way such that the the Tag Rate Matrix prediction is normalized to (CDF data - MC backgrounds).

IV. CONTROL REGIONS

To test our ability to predict the backgrounds, we check the performance of our models in several control regions. The first, the QCD Control Region, is a high statistics region where we check the data-based model.

Since in the Signal Region we expect backgrounds originating from events with real high $\not\!\!E_T$, such as W/Z+jets, $t\bar{t}$ and diboson production, we test our ability to predict these types of backgrounds in a second control region, the Electroweak/Top Control Region. In order to remain unbiased to the Signal Region, we require at least one lepton in the event (all events with leptons are vetoed in the Signal Region). This region is sensitive to ElectroWeak/Top processes, and is used to check the overall shapes and normalizations of the Monte Carlo predictions. It also serves as an additional (but low statistics) check of the QCD model. This region cannot be used to extract any information, since it overlaps with the signal region of other single top analyses.

In order to test the data-driven estimation of QCD multijet production in a more signal-like region, we have defined another control region. This region intends to test the QCD multijet data-based modeling in a kinematic region which is very similar to Signal Region. This region is defined by reversing the QCDNN output cut to remain blind to the signal region. This is also the region from which we extract the normalization of our data-driven QCD multijet production model.

In summary:

- QCD Control Region
  - all leptons are vetoed using loose lepton identifications ;
  - azimuthal angular separation $\Delta\phi(2^{nd}jet, \not\!\!E_T) \leq 0.4$;
  - $\not\!\!E_T > 70$GeV (*50 GeV< $\not\!\!E_T$ <70 GeV region is used to build the TRM for the data-based model*).
- Electroweak/Top Control Region
  - at least one loose lepton is required ;
  - azimuthal angular separation $\Delta\phi(2^{nd}jet, \not\!\!E_T) > 0.4$.
- Signal-like, QCD-rich Control Region
  - all leptons are vetoed using loose lepton identifications ;
  - azimuthal angular separation $\Delta\phi(1^{\text{st}}$ jet, $\not\!\!E_T) \geq 1.5$, $\Delta\phi(2^{\text{nd}}$ jet, $\not\!\!E_T) \geq 0.4$, $\Delta\phi(3^{\text{rd}}$ jet, $\not\!\!E_T) \geq 0.4$;
  - QCDNN < -0.1, to have a high statistics sample where to check the data modeling as well as to extract the multijet normalization scale factor.
- Signal Region
  - $\not\!\!E_T > 50$;
  - all leptons are vetoed using loose lepton identifications ;
  - azimuthal angular separation $\Delta\phi(1^{\text{st}}$ jet, $\not\!\!E_T) \geq 1.5$, $\Delta\phi(2^{\text{nd}}$ jet, $\not\!\!E_T) \geq 0.4$, $\Delta\phi(3^{\text{rd}}$ jet, $\not\!\!E_T) \geq 0.4$;
  - QCDNN > -0.1.

Table II lists the expected and observed event yields in Signal Region.

V. THE SEARCH FOR THE SIGNAL

As mentioned above, we selected the Signal Region to maximize signal significance keeping high signal efficiency. By cutting on the QCDNN, we were able to reduce the main background, QCD multijet events faking high $\not\!\!E_T$, by 77% (the overall background was reduced by 65%) while keeping 91% of the signal. We improved the signal significance ($S/\sqrt{S+B}$) by 50% and the S/B ratio by 150%, from 1/50 to 1/20. At this point, the dominating backgrounds are QCD multijet production, W/Z+jets and ttbar. We studied the dynamic of those events to develop a NN with the goal of discriminating the surviving backgrounds from the interesting signal.

CDF Run II Preliminary, 2.1 fb^{-1}

Process	Excl. SecVTX	SecVTX + SecVTX	SecVTX + JetProb
Single Top S	15.7±2.0	7.6±0.9	6.3±0.8
Single Top T	31.2±4.9	1.7±0.2	1.6±0.2
Top Pair	125±23	30.3±5.8	29.2±5.7
Di-Boson	33.0±6.5	4.9±0.6	4.2±0.6
W + h.f.	269±113	12.7±7.5	22.7±13.7
Z + h.f	105±53	11.8±5.8	11.8±6.0
QCD Multijet	592±27	28.9±3.8	58.5±5.8
Exp. Signal	46.8±5.2	9.3±1.0	7.9±0.8
Exp. Background	1125±169	89±15	126±21
Total Expected	1172±169	98±15	134±21
DATA	1167	113	131

TABLE II: Number of expected and observed events in the Signal Region in all tagging categories.

A. A second NN to discriminate the signal from the backgrounds

We again train a MLP as implemented in TMVA. This time, we use the single top s- and t-channels in their respective proportions, which is also what we do with all the background processes accounting for more that 5% of the total background, i.e. pre-tag data times tag rate probability (for modeling QCD multijet), top pair, $W \to \tau\nu$ and $Z \to \nu\nu$.

We use the following 11 variables in our NN:

- Invariant mass of the second jet and missing transverse energy; the second jet in the $W \to \tau\nu$ events is often a τ, thus this variable is the reconstructed W transverse mass for the background events;
- Scalar sum of transverse energy of the two or three leading jets, H_T^3;
- Minimum of the difference in ϕ between the $\not\!\!E_T$ and each jet j_i, considering all two or three $(\not\!\!E_T, j_i)$ pairings;
- Z$(j_{1(2)})$: Ratio of the sum of Pass 1 track P_Ts to the $P_T(j_{1(2)})$;
- Absolute amount of the missing transverse energy, $\not\!\!E_T$;
- Absolute amount of the missing transverse momentum, $\not\!\!P_T^{tr}$;
- $\Delta\phi$ between the direction of the leading jets in two-jet rest frame and the direction of the boost;
- $\not\!\!E_T/H_T$;
- Invariant mass of $\not\!\!E_T$, j_1 and j_2;
- Invariant mass of all tight jets in the event, m_{3j};

The output of this NN, which we call the final NN discriminant, is shown in figure 3. The distributions of the input variables are shown in the Signal Region for all tagging categories on the CDF public web-page of this analysis [10]. The final NN discriminant output is also shown there for each Control Region.

B. Systematic Uncertainties

Systematic uncertainties are split in normalization uncertainty and shape uncertainty. The normalization uncertainty reflects changes to the event yield due to the systematic effect while the shape uncertainty reflect changes to the template histograms. Both of these effects can be included, depending on the source the systematic uncertainty.

The systematic uncertainties are also classified as correlated and uncorrelated errors considering the relations between the signal and the background processes. The correlated errors are taken into account separately for each processes in the limit calculation. The uncorrelated systematic uncertainties are: QCD multi-jet normalization, MC statistical uctuations. Additionally, the statistical variations in TRM, which is used to estimate the multijet

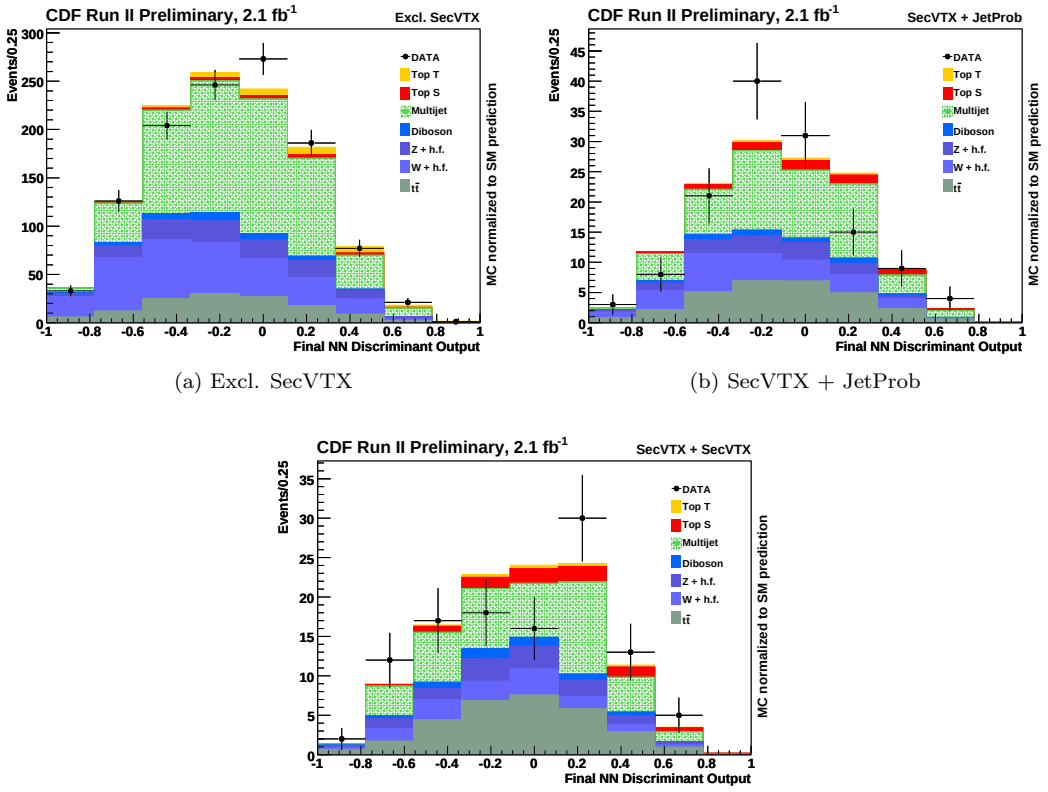

(a) Excl. SecVTX

(b) SecVTX + JetProb

(c) SecVTX + SecVTX

FIG. 3: Final NN discriminant output distribution in Signal Region

background, can also modify the shape of the distributions. It is taken into account by varying the TRM probability in each bin of the matrix by $\pm 1\sigma$, and the alternative shapes are used in the cross-section calculation. The correlated systematics are: luminosity, b-tagging efficiency scale factor between data and Monte Carlo, trigger efficiency, lepton veto efficiency, PDF uncertainty and Jet Energy Scale. ISR/FSR systematic uncertainties and top mass dependence uncertainty, considering top masses of 170 and 180 GeV as $\pm 2\sigma$ variations, are applied on the top processes. We include an uncertainty due to the contamination by the signal when estimating the QCD multijet production from data. To do so, we vary the amount of single top we subtract from the QCD multijet prediction by 50%. Also, because of the overlap in data and MC events we have with the other CDF analyses, we have scaled down the background by 2% and assigned a systematic uncertainty of 2%. Finally, to compute the p-value and V_{tb}, we consider the theoretical uncertainty on the single top production cross-section.

The systematic uncertainties are summarized in Table III.

C. Results

Comparisons of the distributions of the neural network outputs for all tagging categories in all Control Regions and in the Signal Region are shown on the CDF public web-page of the analysis [10].

We use a likelihood profile [11] of this discriminant to measure the production cross section of single top events. Once we apply our analysis to the first 2.1 fb^{-1} of data recorder by CDF II, we expect a single top cross-section of

$$\sigma_{s+t}^{exp} = 2.7^{+2.3}_{-2.1} \text{ pb}.$$

We measure a single top production cross-section of

$$\sigma_{s+t}^{obs} = 4.9^{+2.5}_{-2.2} \text{ pb}.$$

We also perform the measurement in each tagging category separated. The results are shown in figure 4.

Systematic	Rate	Shape	Comment
Luminosity	6%	-	Not for QCD multijet
PDF	+0.7% / -0.4% (s-chan)	X	
	+2.3% / -2.1% (t-chan)	X	
	+0.8% / -1.4% (top pair)	-	
	2% (MC backgrounds)	-	
JES	-13.9% ... 23%	X	
QCD multijet normalization	4.5% (ST)	-	Only QCD multijet
	13.1% (ST + ST)	-	
	10.0% (ST + JP)	-	
B tagging	4.3% (ST)	-	
	8.6% (ST + ST)	-	
	12.3% (ST + JP)	-	
W & Z + h.f. cross-section	40%	-	
Di-bonson cross-section	11.5%	-	
Top pair cross-section	±12.4%	-	
Trigger Efficiency	±0% ... ± 2.6%	X	Not for QCD multijet
Lepton Veto	2%	-	
ISR/FSR	-4.5% ... 16.5%	X	Only top-processes
Top mass dependence	-16.4% ... 7.5%	X	Top mass only for V_{tb} and p-value
TRF	-	X	Only QCD multijet
Signal contamination	-	X	Only QCD multijet
Background scaling	2%	-	
Signal cross-section	± 12.4% (s-chan)	-	Only for p-value and V_{tb}
	± 12.6% (t-chan)	-	

TABLE III: Summary of systematics

Using a test statistic, we compute the probablility that the background model (B) fluctuated equal or up to the observed value in the data (observed p-value) or to the median of signal plus background (S+B) pseudo-experiments (expected p-value). We obtain an expected p-value of 0.0785 (1.4σ) and an observed p-value of 0.0160 (2.1σ). The results are shown in figure 5.

Finally, we measure the V_{tb} element of the CKM matrix to be $|V_{tb}| = 1.24^{+0.34}_{-0.29} \pm 0.07$(theory) (see figure 6).

VI. SUMMARY

We have presented a search for s- and t-channel electroweak single top production in the $\not\!\!E_T$+jets channel. We have analyzed 2.1 fb^{-1} of CDF Run II data and measured the single top production cross-section for the first time in this channel (events where the lepton from the W decay is either not identified or reconstructed as a jet). We find, assuming a top quark mass of 175 GeV/c^2,

$$\sigma^{obs}_{s+t} = 4.9^{+2.5}_{-2.2} \text{ pb.}$$

The observed p-value is 0.0160 (2.1 σ). Finally, we have measured the V_{tb} element of the CKM matrix :

$$|V_{tb}| = 1.24^{+0.34}_{-0.29} \pm 0.07\text{(theory)}.$$

Acknowledgments

We thank the Fermilab staff and the technical staffs of the participating institutions for their vital contributions. This work was supported by the U.S. Department of Energy and National Science Foundation; the Italian Istituto Nazionale di Fisica Nucleare; the Ministry of Education, Culture, Sports, Science and Technology of Japan; the Natural Sciences and Engineering Research Council of Canada; the National Science Council of the Republic of China; the Swiss National Science Foundation; the A.P. Sloan Foundation; the Bundesministerium fuer Bildung und Forschung, Germany; the Korean Science and Engineering Foundation and the Korean Research Foundation; the Particle Physics and Astronomy Research Council and the Royal Society, UK; the Russian Foundation for Basic

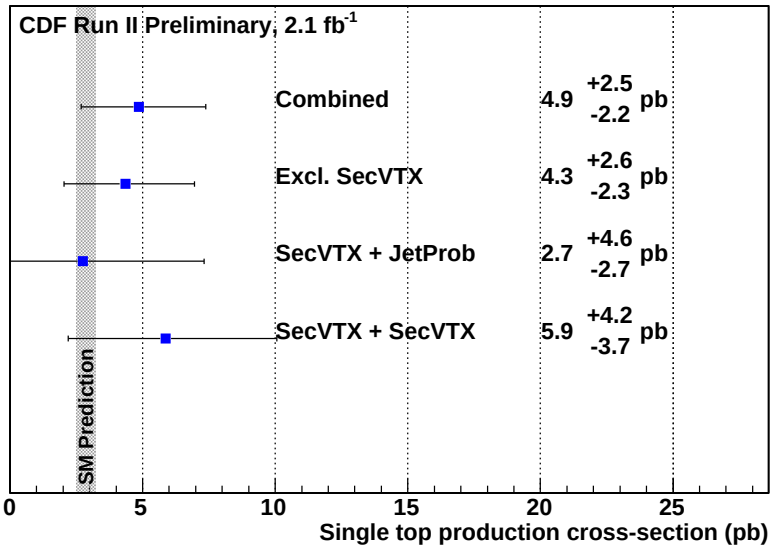

FIG. 4: Measurement of the single top cross-section production. We show the result in each of our tagging categories as well as their combination.

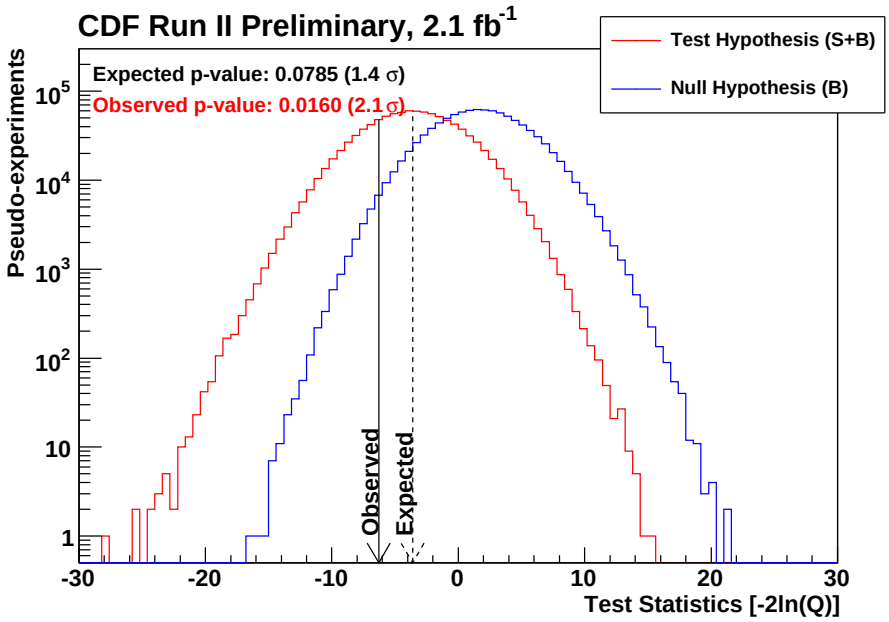

FIG. 5: Test statistics for expected cross-section measurement.

Research; the Comision Interministerial de Ciencia y Tecnologia, Spain; and in part by the European Community's Human Potential Programme under contract HPRN-CT-20002, Probe for New Physics.

[1] B. W. Harris, et al., Phys. Rev. D, 66, 054024, 2002; Z. Sullivan, Phys. Rev. D, 70, 114012, 2004; N.Kidonakis, Phys. Rev. D, 74, 114012, 2006

[2] F. Abe, et al., Nucl. Instrum. Methods Phys. Res. A **271**, 387 (1988); D. Amidei, et al., Nucl. Instum. Methods Phys. Res.

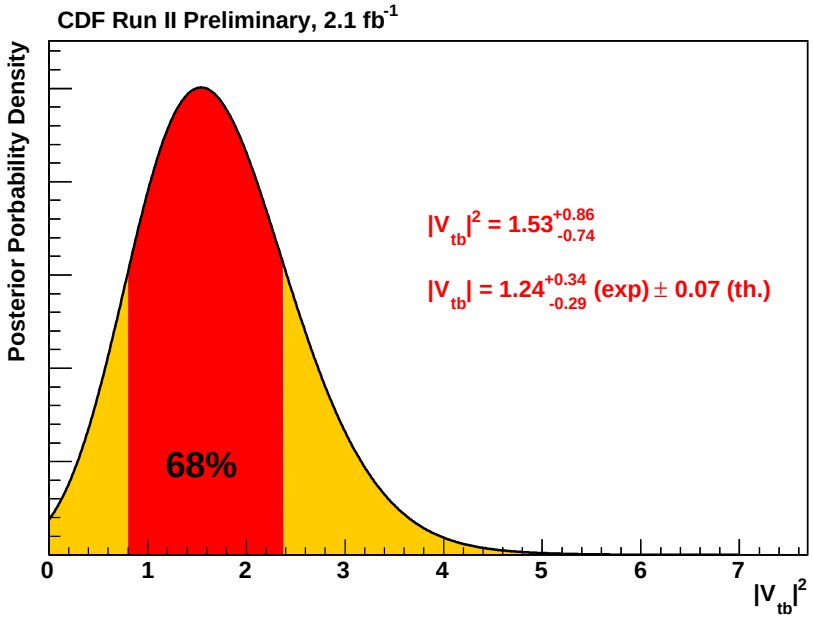

FIG. 6: Measurement of the V_{tb} element of the CKM matrix.

A **350**, 73 (1994); F. Abe, et al., Phys. Rev. D **52**, 4784 (1995); P. Azzi, et al., Nucl. Instrum. Methods Phys. Res. A **360**, 137 (1995); The CDFII Detector Technical Design Report, Fermilab-Pub-96/390-E
[3] CDF Collaboration, Phys. Rev. D 76, 072010 (2007)
[4] H1 Collaboration, C. Adlo et al., Z. Phys. C74 (1997) 221.
[5] A. Acosta et al., Phys. Rev. D 71, 052003 (2005)
[6] A. Abulencia et al., Phys. Rev. D 74, 072006 (2006)
[7] A. Hocker et al., arXiv:physics/0703039.
[8] T. Sjostrand et al., Comput. Phys. Commun. **135**, 238 (2001).
[9] M. Cacciari, et al., JHEP, 09 (127), 2008, arXiv:0804.2800 [hep-ex].
[10] `http://www-cdf.fnal.gov/physics/new/top/2008/singletop/METbb/`
[11] T. Junk, CDF/DOC/STATISTICS/PUBLIC/8128.